



HAL
open science

Kinetic and thermodynamic analysis of Cu^{2+} -dependent reductive inactivation in direct electron transfer-type bioelectrocatalysis by copper efflux oxidase

Taiki Adachi, Ievgen Mazurenko, Nicolas Mano, Yuki Kitazumi, Kunishige Kataoka, Kenji Kano, Keisei Sowa, Elisabeth Lojou

► To cite this version:

Taiki Adachi, Ievgen Mazurenko, Nicolas Mano, Yuki Kitazumi, Kunishige Kataoka, et al.. Kinetic and thermodynamic analysis of Cu^{2+} -dependent reductive inactivation in direct electron transfer-type bioelectrocatalysis by copper efflux oxidase. *Electrochimica Acta*, 2022, 429, pp.140987. 10.1016/j.electacta.2022.140987 . hal-03752803

HAL Id: hal-03752803

<https://hal.science/hal-03752803>

Submitted on 17 Aug 2022

HAL is a multi-disciplinary open access archive for the deposit and dissemination of scientific research documents, whether they are published or not. The documents may come from teaching and research institutions in France or abroad, or from public or private research centers.

L'archive ouverte pluridisciplinaire **HAL**, est destinée au dépôt et à la diffusion de documents scientifiques de niveau recherche, publiés ou non, émanant des établissements d'enseignement et de recherche français ou étrangers, des laboratoires publics ou privés.

1
2
3 **Kinetic and thermodynamic analysis of Cu²⁺-dependent reductive inactivation in**
4
5 **direct electron transfer-type bioelectrocatalysis by copper efflux oxidase**
6
7

8
9
10 Taiki Adachi^{a,b*}, Ievgen Mazurenko^a, Nicolas Mano^c, Yuki Kitazumi^b, Kunishige
11
12 Kataoka^d, Kenji Kano^e, Keisei Sowa^b, and Elisabeth Lojou^a
13
14

15
16
17 a) *Aix Marseille University, CNRS, BIP, Bioénergétique et Ingénierie des Protéines, 31*
18
19 *chemin Aiguier, 13402 Marseille, France*
20

21
22 b) *Division of Applied Life Sciences, Graduate School of Agriculture, Kyoto University,*
23
24 *Sakyo, Kyoto 606-8502, Japan*
25

26
27 c) *Centre de Recherche Paul Pascal (CRPP), UMR 5031, CNRS, University of Bordeaux,*
28
29 *33600 Pessac, France*
30

31
32 d) *Division of Material Sciences, Graduate School of Natural Science and Technology,*
33
34 *Kanazawa University, Kakuma, Kanazawa 920-1192, Japan*
35

36
37 e) *Center for Advanced Science and Innovation, Kyoto University, Gokasho, Uji, Kyoto*
38
39 *611-0011, Japan*
40

41
42
43 *Corresponding author: Mr. Taiki Adachi
44

45
46 *E-mail address:* adachi.taiki.62s@st.kyoto-u.ac.jp
47
48

49
50
51 *Keywords:*

52
53 Multicopper oxidase

54
55 Copper efflux oxidase

56
57 Direct electron transfer
58
59

1
2
3 Bioelectrochemistry

4
5 Cu²⁺ effects
6
7
8
9

10 **Abstract**

11
12 Copper efflux oxidases (CueOs) are key enzymes in copper homeostasis systems.
13
14 The mechanisms involved are however largely unknown. CueO-type enzymes share a
15 typical structural feature composed of Methionine-rich (Met-rich) domains that are
16 proposed to be involved in copper homeostasis. Bioelectrocatalysis using CueO-type
17 enzymes in the presence of Cu²⁺ recently highlighted a new Cu²⁺-dependent catalytic
18 pathway related to a cuprous oxidase activity. In this work, we further investigated the
19 effects of Cu²⁺ on direct electron transfer (DET)-type bioelectrocatalytic reduction of O₂
20 by CueO at NH₂-functionalized multi-walled carbon nanotubes. The DET-type
21 bioelectrocatalytic activity of CueO decreased at low potential in the presence of Cu²⁺,
22 showing unique peak-shaped voltammograms that we attribute to inactivation and
23 reactivation processes. Chronoamperometry was used to kinetically analyze these
24 processes, and the results suggested linear free energy relationships between the
25 inactivation/reactivation rate constant and the electrode potential. Pseudo-steady-state
26 analysis also indicated that Cu²⁺ uncompetitively inhibited the enzymatic activity. A
27 detailed model for the Cu²⁺-dependent reductive inactivation of CueO was proposed to
28 explain the electrochemical data, and the related thermodynamic and kinetic parameters.
29
30 A CueO variant with truncated copper-binding α helices and bilirubin oxidase free of Met-
31 rich domains also showed such reductive inactivation process, which suggests that
32 multicopper oxidases contain copper-binding sites that lead to inactivation.
33
34
35
36
37
38
39
40
41
42
43
44
45
46
47
48
49
50
51
52
53
54
55
56
57
58
59
60
61
62
63
64
65

1. Introduction

Multicopper oxidases (MCOs) are essential enzymes in many organisms and have been widely studied in the biochemistry, electrochemistry, and spectroscopy fields [1,2]. In solution, substrates such as phenols, bilirubin, and ascorbate are oxidized at type I (T1) Cu, and the extracted electrons are transferred to the trinuclear copper cluster (TNC) composed of one type II (T2) Cu and two type III (T3) Cu moieties, where dioxygen (O₂) is reduced into water [1,2]. MCOs are often utilized as O₂-reducing cathodic catalysts for bioelectrochemical applications, such as O₂ biosensors and biofuel cells [3,4]. They can undergo enzymatic reactions on electrode materials that act as electron donors and react with the T1 Cu. Such direct electrical communication between an enzyme and an electrode is called direct electron transfer (DET)-type bioelectrocatalysis [5–9]. For such purposes, carbon nanotube (CNT) networks are widely used as efficient platforms for DET-type bioelectrocatalysis of various enzymes including MCOs [10–13].

Copper efflux oxidase (CueO) belongs to the MCO family. It is supposed to be able to protect periplasmic enzymes from copper mediated toxicity by oxidizing the harmful cuprous ion (Cu⁺) [14–17]. Consequently, CueO is proposed to play an important role as a radical scavenger in bacterial copper homeostasis, although the exact mechanism is largely unknown. *Escherichia coli* (*E. coli*) CueO has been the most studied among CueO-type enzymes. Unlike other MCOs such as laccase (Lac) or bilirubin oxidase (BOD), the uniqueness of the *E. coli* CueO structure is associated with a large segment composed of α helices (helices 5, 6, and 7 from the N-terminus) that cover the T1 Cu site, which results in low catalytic activity toward the oxidation of large electron-donating substrates such as 2,2'-azinobis(3-ethylbenzothiazoline-6-sulfonic acid) (ABTS) [18,19].

1
2
3 In contrast, the helical region provides additional copper-binding sites; consequently,
4
5 ABTS-oxidizing activity is improved in the presence of excess cupric ion (Cu^{2+}), because
6
7 the bound coppers mediate the electron transfer between ABTS and the T1 Cu [18–20].
8
9
10 In bioelectrocatalysis, on the other hand, *E. coli* CueO exhibits strong DET-type activity
11
12 on positively charged electrodes because the surface charge near the T1 Cu site is negative
13
14 [21]. Hence, positively charged platforms can electrostatically control the enzyme
15
16 orientation in a manner favorable for the interfacial electron transfer from the electrode
17
18 to the T1 Cu [21].
19
20
21

22 Our group recently studied the bioelectrocatalytic reduction of O_2 by Lac from
23
24 *Thermus thermophilus* (TtLac). TtLac structure shows a copper-binding Met-rich hairpin
25
26 domain near the T1 Cu, thus presenting similarity with *E. coli* CueO [22]. As with *E. coli*
27
28 CueO, modification of electrodes by positively charged CNTs were found to be favorable
29
30 for DET, while negative ones prevented DET process. For the first time, it was however
31
32 demonstrated that addition of Cu^{2+} allowed bioelectrocatalytic O_2 reduction at negative
33
34 CNTs, at a potential lower than the expected potential for a catalytic process passing
35
36 through the T1 Cu, hence suggesting a change in the electron transfer pathway between
37
38 the enzyme and the electrode. The process was tentatively attributed to the cuprous
39
40 oxidase activity of the enzyme induced by Cu binding to the Met-rich domain. On
41
42 positively charged CNTs where DET was favored, Cu^{2+} addition induced progressive
43
44 DET current decrease with simultaneous occurrence of the Cu^{2+} -related catalytic wave.
45
46
47
48
49
50
51 Whatever positive or negative CNTs-based electrodes, voltammograms recorded in the
52
53 presence of Cu^{2+} were peak-shaped. While the cause of this observation remained
54
55 unknown, it was suggested that Cu^{2+} -related electrocatalytic activation may be
56
57 accompanied by an inactivation process. MCO inhibition by H_2O_2 and halides have been
58
59
60
61
62
63
64
65

1
2
3 reported [23–28]. As far as we know, MCO inactivation by Cu^{2+} was never reported.
4

5 In this study, with the final objective of improving the understanding of copper
6 homeostasis, we examined how Cu^{2+} affects the bioelectrocatalytic properties of CueO,
7 with a special focus on the inactivation caused by Cu^{2+} . We especially analyzed kinetic
8 data in order to discuss a potential inhibition mechanism. In addition, we investigated
9 how the helical structure affects the bioelectrocatalytic properties of wild-type CueO by
10 comparing it with its variant lacking Met-rich α helices and another MCO lacking any
11 Met-rich domains.
12
13
14
15
16
17
18
19
20
21
22
23

24 **2. Experimental**

25 **2.1. Materials and chemicals**

26
27
28
29 Recombinant wild-type CueO (rCueO) and its variant truncating α helices 5 to 7
30 ($\Delta\alpha$ CueO) were expressed in *E. coli* and purified according to the literature procedure
31 [18]. BOD from *Bacillus pumilus* (BpBOD) was purified according to the literature
32 procedure [29]. Multi-walled CNTs (MWCNTs) functionalized with $-\text{NH}_2$ groups (CNT-
33 NH_2 ; diameter: 10 nm, length: 1.5 μm) and $-\text{COOH}$ groups (CNT-COOH; diameter: 15
34 nm, length 5–20 nm) were obtained from Metrohm Dropsens (Spain) and NanoLab Inc.
35 (USA), respectively. MWCNTs without any functionalization (nCNT; diameter: 9.5 nm,
36 length: 1.5 μm) were obtained from Nanocyl SA (Belgium). All other reagents were
37 purchased from Sigma–Aldrich (Merck, Germany). All solutions were prepared using
38 ultrapure water.
39
40
41
42
43
44
45
46
47
48
49
50
51
52
53
54

55 **2.2. Electrode preparation**

1
2
3 Planar glassy carbon electrodes (GCs; diameter: 3 mm) were polished with an
4 alumina slurry, sonicated and washed with distilled water. Then, CNT-NH₂ or nCNT
5 slurry dispersed in *N*-methyl-2-pyrrolidone was applied onto the surface of GCs and dried
6 under reduced pressure. The amount of deposited CNT-NH₂ and nCNT was set to 0.5 μg
7 and 5 μg, respectively. These electrodes are referred to as CNT-NH₂/GCs and nCNT/GCs,
8 respectively. On the other hand, a CNT-COOH slurry dispersed in water was applied onto
9 the surface of GCs and dried under reduced pressure. The amount of deposited CNT-
10 COOH was set to 5 μg. These electrodes are referred to as CNT-COOH/GCs. A 5-μL
11 aliquot of a 20 μM enzyme solution dissolved in 0.1 M phosphate buffer (pH 7.0) was
12 then applied to CNT-NH₂/GC, nCNT/GC, and CNT-COOH/GC, after which the
13 electrodes were placed in a water-saturated atmosphere for 2 h at 4 °C. The enzyme-
14 modified electrodes were washed with buffer solution before electrochemical
15 measurements.

36 **2.3. Electrochemical measurements**

37
38 All electrochemical measurements were performed at 25 °C using a potentiostat
39 (PGSTAT302N) and a rotating electrode instrument (RRDE) controlled by Nova 2.0
40 software (Metrohm Autolab, Switzerland). The rotation speed (ω) of the working
41 electrode was set to 4000 rpm. Platinum wire and a Hg|Hg₂SO₄|sat. K₂SO₄ electrode were
42 used as counter and reference electrodes, respectively. In this study, all potentials were
43 converted into potentials against the standard hydrogen electrode (SHE) by adding 0.64
44 V to the measured potential. 0.1 M acetate buffer at pH 5.0 was used as the electrolyte
45 solution. The atmosphere was controlled by continuously bubbling either O₂ or N₂ gas
46 into the buffer.

2.4. Circular dichroism (CD) spectroscopy

20 μM of proteins in 10 mM acetate buffer (pH 6.0) were analyzed by far-UV CD spectroscopy using a J-715 spectropolarimeter (Jasco, Japan) at 25 °C in a cell with a 0.5-mm path-length. Spectra from an average of 10 accumulated scans were acquired.

3. Results and discussion

3.1. Effects of Cu^{2+} on DET-type O_2 reduction by CueO

Cyclic voltammograms (CVs) recorded for the enzyme-modified CNT-NH₂/GCs are shown in Fig. 1. Clear reversible and sigmoidal waves ascribed to DET-type O_2 reduction catalyzed by rCueO and $\Delta\alpha\text{CueO}$ were observed in an O_2 -saturated atmosphere (broken lines in Figs. 1A and B, respectively). CuSO_4 was then added to the buffer solution. As the CuSO_4 concentration increased, and as the overpotential increased, the catalytic current density clearly decreased at both the rCueO- and $\Delta\alpha\text{CueO}$ -modified electrodes, with the occurrence of peak shaped curves (solid lines in Figs. 1A and B, respectively). The irreversibility observed between the forward and reversed scans in each voltammogram also reveals that Cu^{2+} induces kinetic hysteresis in the DET-type O_2 reduction by CueO, which indicates that the Cu^{2+} -dependent process is more slowly than the change in the electrode potential. CVs were recorded at various scan rates (Fig. 2). As the scan rate slowed down, the peak shape was more and more evident. Similar changes in the shapes of the CVs were observed in a study relative to the oxidative inactivation in DET-type bioelectrocatalysis of the O_2 -tolerant [NiFe]-hydrogenase [30,31]. By homology, we will refer to “reductive inactivation” to reflect the effects of Cu^{2+} on CueO bioelectrocatalysis.

1
2
3 We previously reported similar abovementioned CV shapes in the case of O₂
4 reduction by *TiLac* immobilized on the same CNT-NH₂ [22]. It could thus be
5 hypothesized that such Cu²⁺-dependent inactivation is specific to CueO-like enzymes
6 presenting Met-rich domains covering the T1 Cu. However, the inactivation process was
7 also observed using *BpBOD*, another MCO lacking such domains (Fig. S1). Structural
8 alignments of CueO, *BpBOD*, and *TiLac* proved their high homology (Figs. S2 and S3).
9 While the structure of the three cupredoxin domains and general fold might be the same,
10 the additional Met-rich domain is missing in *BpBOD*. Thus, we concluded that the Cu²⁺-
11 dependent inactivation is not related to the Met-rich domain.
12
13
14
15
16
17
18
19
20
21
22
23

24 The addition of other divalent metal cations (Ca²⁺ and Ni²⁺) did not result in such
25 a decrease in current (Fig. S4), from which we can conclude that the Cu²⁺-dependent
26 inactivation in CueO bioelectrocatalysis is not due to any electrostatic interactions caused
27 by additional ions. In addition, the rCueO-modified nCNT/GC also showed similar
28 behavior to the rCueO-modified CNT-NH₂/GC for Cu²⁺ (Fig. S5), which suggests that
29 NH₂ functional groups at MWCNTs are not involved in the Cu²⁺-dependent inactivation
30 process.
31
32
33
34
35
36
37
38
39
40

41 In addition, the involvement of MCOs potentially depleted of the T2 Cu can be
42 ruled out [32–35]. Indeed, since only the catalytic current produced by active enzymes
43 was measured, the presence or absence of the fraction without the T2 Cu do not interfere
44 with the analysis. Furthermore, both DET-type and ABTS-oxidizing activities of CueO
45 were stable for a long while, suggesting that the T2 Cu was maintained in the enzyme and
46 its mobility can be negligible.
47
48
49
50
51
52
53
54

55 Cu²⁺ is electrochemically active on a carbon electrode. The formal potentials of
56 the Cu²⁺/Cu⁰ and Cu²⁺/Cu⁺ redox couples are 0.340 V and 0.159 V, respectively [36],
57
58
59
60
61
62
63
64
65

1
2
3 without consideration of complexation with other ions (acetate in this case). Hence, direct
4
5 electrochemical reactions involving Cu species may interfere with reductive inactivation
6
7 of CueO. 1-Electron reduction from Cu^{2+} to Cu^+ appears to be negligible since the
8
9 reaction is thermodynamically unfavorable under normal conditions due to the instability
10
11 of Cu^+ devoid of desirable ligands in aqueous solution. We recorded multi-scanned CVs
12
13 swept down to two different cathodic potentials, namely 0.3 V and 0.2 V. Cu^{2+} -dependent
14
15 reductive inactivation was observed to be reversible during three cycles when the lowest
16
17 potential was set to 0.3 V (Fig. 3A). In this potential range, redox currents relative to Cu^{2+}
18
19 were hardly distinguishable from the background (dotted red lines in Fig. 3A). At the
20
21 abiotic CNT-NH₂/GC in the presence of 1 mM CuSO_4 , Cu^{2+} reduction to Cu^0 starts to be
22
23 involved at lower potentials than 0.3 V, as denoted by the anodic redissolution peak
24
25 clearly seen in Fig. S6. These results suggest that the reductive inactivation of CueO is
26
27 not ascribed to direct Cu^{2+} reduction at the electrode, but to some interaction between the
28
29 enzyme and Cu^{2+} inducing catalysis. In contrast, current density was observed to
30
31 irreversibly decrease with continuous scanning when the lowest potential was set to 0.2
32
33 V (Fig. 3B). Considering that the background cathodic current appeared from 0.3 V
34
35 (dotted red lines in Fig. 3B), the irreversible decrease in current observed during
36
37 continuous scanning may be due to the electrodeposition of Cu metal at the electrode
38
39 surface, which may interfere with the enzyme–electrode interface.
40
41
42
43
44
45
46
47

48 As mentioned in the introduction, Cu^{2+} reportedly enhances rCueO activity for
49
50 ABTS oxidation in solution most probably through coordination near helices 5–7 [19].
51
52 Such enhancement was also observed in DET-type reactions at negatively charged CNTs
53
54 (CNT-COOH) for rCueO (Fig. S7), in a similar manner to that described previously for
55
56 *Tt*Lac. It was ascribed to an electron transfer pathway from the additional copper-binding
57
58
59
60
61
62
63
64
65

1
2
3 site to the T1 Cu. However, such enhancement was not observed for both the rCueO- and
4
5 $\Delta\alpha$ CueO-modified CNT-NH₂/GCs, most likely because the enzyme is favorably oriented
6
7 to promote DET between the T1 Cu and the electrode. In agreement with this assumption,
8
9 Cu²⁺-related waves progressively occurred at the CNT-NH₂-based electrode for *TtLac*
10
11 which showed a lower DET-type current than rCueO [22].
12
13

14
15 On the other hand, Cu²⁺-dependent reductive inactivation was not observed in
16
17 the solution reaction, as the addition of Cu²⁺ reportedly enhances CueO activity [18]. The
18
19 difference in CueO behavior between DET-type bioelectrocatalysis and the solution
20
21 reaction can be explained from thermodynamic viewpoints. The formal potentials of the
22
23 electron donors used for assaying CueO activities (e.g., the formal potential of ABTS^{1-/2-}
24
25 is 0.63 V at pH 5.3 [37]) appear to be too positive to observe Cu²⁺-dependent reductive
26
27 inactivation, which was clearly observed at potentials below approximately 0.4 V. This
28
29 assumption is also in agreement with our previous observation that a mutant of *TtLac*
30
31 with a 100 mV higher potential was indeed inactivated by the addition of Cu²⁺ in solution
32
33 [38].
34
35
36
37
38
39
40

41 **3.2. Kinetic analysis of Cu²⁺-dependent reductive inactivation**

42
43 In this section, we analyze the kinetics of Cu²⁺-dependent reductive inactivation
44
45 of DET-type bioelectrocatalysis by CueOs according to previous reports on [NiFe]-
46
47 hydrogenase [30,31,39]. First, reversible (bi-directional) inactivation and reactivation are
48
49 simply expressed by pseudo-first-order reversible kinetics, as follows:
50
51



58 where E_A and E_I are enzymes in the active and inactive states, respectively, and k_I and k_A

are the apparent reaction kinetic constants for inactivation and reactivation, respectively. This kinetic equation can be solved for the surface concentration of E_A ($= [E_A]$), and the catalytic current density (j_{cat}) linearly depends on $[E_A]$. Thus, j_{cat} is expressed as follows [31]:

$$j_{cat} = j_0 \left\{ \frac{k_I}{k_I + k_A} \exp[-(k_I + k_A)t] + \frac{k_A}{k_I + k_A} \right\} \quad (2)$$

where t is time and j_0 is j_{cat} at $t = 0$.

On the other hand, the apparent limiting current density (j_{app}) at a rotating disk electrode is expressed by Koutecký–Levich equation:

$$\frac{1}{j_{app}} = \frac{1}{j_{mt}} + \frac{1}{j_{cat}} \quad (3)$$

where j_{mt} is the current density controlled by the mass transfer of the substrate (O_2), and is expressed by Levich equation:

$$j_{mt} = -0.62n_{O_2}FD_{O_2}^{\frac{2}{3}}\nu^{-\frac{1}{6}}c_{O_2}\omega^{\frac{1}{2}} \quad (4)$$

where n_{O_2} , F , D_{O_2} , ν , and c_{O_2} are the number of electrons of O_2 reduction ($= 4$), the Faraday constant, the diffusion constant of O_2 ($= 2.0 \times 10^{-5} \text{ cm}^2 \text{ s}^{-1}$ at $25 \text{ }^\circ\text{C}$ [40]), the kinematic viscosity of the buffer ($= 0.009 \text{ cm}^2 \text{ s}^{-1}$ at $25 \text{ }^\circ\text{C}$ [41]), and the bulk concentration of O_2 ($= 1.2 \text{ mM}$ at $25 \text{ }^\circ\text{C}$ under O_2 -saturated conditions [42]), respectively. Thus, j_{mt} is calculated to be -9.5 mA cm^{-2} under O_2 -saturated conditions at $\omega = 4000 \text{ rpm}$.

In the following analysis, we considered the contribution of j_{mt} and converted the experimentally measured j_{app} into j_{cat} by Eq. (3). Using k_I and k_A as adjustable parameters, Eq. (2) was fitted to chronoamperograms (CAs) by non-linear regression analysis using Gnuplot[®]. To simplify the model, j_0 was considered to be equal to the value of j_{cat} measured in each CA prior to the addition of $CuSO_4$. To neglect interference of the charging current, experimental data acquired in the 0–1 s range were removed prior to

1
2
3 analysis. All CAs were recorded after the working electrode was set to 0.8 V for 30 s to
4
5 completely reactivate enzymes. The fitted results are shown in Figs. 4 and S8, and the
6
7 refined values of k_I and k_A are shown in Figs. S9 and S10. The collected data are
8
9 summarized in Fig. 5 to facilitate a simple comparison of rCueO and $\Delta\alpha$ CueO.
10

11
12 Linear free energy relationships between the potential and the common
13
14 logarithms of k_I and k_A were observed to some extent (Figs. 5A and 5B), which suggests
15
16 that k_I and k_A partly obey the Butler–Volmer equation. Partial non-linearity especially
17
18 shown in $\log(k_I / \text{s}^{-1})$ vs. E plots is probably due to the small contribution of the Butler–
19
20 Volmer equation in the analyzed potential range. In contrast, k_I clearly showed a
21
22 proportional relationship with the Cu^{2+} concentration (Fig. 5C), whereas k_A is less
23
24 dependent on the Cu^{2+} concentration (Fig. 5D). These results indicate that inactivation
25
26 and activation are induced by the coordination and dissociation processes of a single Cu^{2+}
27
28 ion, respectively, and that k_I is more contributed by the Cu^{2+} coordination than the Butler–
29
30 Volmer equation in this range of the potential and the Cu^{2+} concentration. However, these
31
32 relationships were not observed under all measurement conditions (Figs. S9 and S10);
33
34 hence, the reductive inactivation of CueO cannot be completely explained using the
35
36 simplest model (Eq. (1)). In addition, we could not find clear differences between rCueO
37
38 and $\Delta\alpha$ CueO from the kinetic viewpoints.
39
40
41
42
43
44
45
46
47

48 **3.3. Discussion on inhibition mechanism**

49

50 We investigated the inhibition mechanism of CueO by Cu^{2+} . It is well-known
51
52 that inhibition mechanisms of enzymes can be estimated from steady-state reaction
53
54 kinetics at variable concentrations of substrate and inhibitor. Accordingly, we recorded
55
56 CAs at the rCueO- and $\Delta\alpha$ CueO-modified CNT-NH₂/GCs at different O₂ and Cu^{2+}
57
58
59
60
61
62
63
64
65

1
2
3 concentrations (c_{O_2} and $c_{\text{Cu}^{2+}}$, respectively), and calculated j_{cat} by considering various j_{mt}
4
5 values. We subsequently assumed that steady-state conditions were achieved at $t = 30$ s;
6
7 hence, we plotted j_{cat}^{-1} values at $t = 30$ s as functions of $c_{\text{O}_2}^{-1}$ and $c_{\text{Cu}^{2+}}$, respectively (Figs.
8
9 6, S11, and S12). j_{cat}^{-1} values calculated under low O_2 concentrations included large errors,
10
11 which are probably due to the large contribution of the mass transfer of O_2 that provides
12
13 mathematical errors for Koutecký–Levich equation. Both Lineweaver–Burk and Dixon
14
15 plots partly showed some parallelism, which suggests uncompetitive inhibition in which
16
17 the inhibitor binds to the enzyme–substrate (ES) complex [43,44]. In contrast, parallelism
18
19 was not clearly observed at $E = 0.3$ V in the presence of 0.5 mM or higher Cu^{2+} (Figs.
20
21 S11A, S11B, S12A, and S12B), which is plausibly due to irreversible enzyme
22
23 denaturation by the electrodeposition of Cu metal at low potentials.
24
25
26
27
28

29
30 Based on previous discussion and results of the kinetic analysis, the
31
32 characteristics of the Cu^{2+} -dependent reversible reductive inactivation and oxidative
33
34 reactivation in CueO bioelectrocatalysis are summarized as follows: 1) both rates of
35
36 inactivation and reactivation are exponentially related to the electrode potential, 2) the
37
38 rate of inactivation is linearly related to $c_{\text{Cu}^{2+}}$, 3) the rate of reactivation is independent of
39
40 $c_{\text{Cu}^{2+}}$, and 4) Cu^{2+} binds the ES complex. Accordingly, we propose the detailed model
41
42 shown in Scheme 1 for the Cu^{2+} -dependent reversible reductive inactivation and oxidative
43
44 reactivation observed in CueO bioelectrocatalysis.
45
46
47

48
49 Here, we assume that the inactivation/reactivation cycle can be divided into non-
50
51 electrochemical and electrochemical processes; the former corresponds to
52
53 coordination/dissociation between the ES complex and Cu^{2+} , while the latter corresponds
54
55 to reduction/oxidation of the ES- Cu^{2+} complex. In addition, the complex of ES and $\text{Cu}^{2+/1+}$
56
57 was assumed to have an active oxidized state (ES- Cu^{2+}) and an inactive reduced state
58
59
60
61
62
63
64
65

(ES-Cu⁺). In this model, the steady-state catalytic current density ($j_{\text{cat,s}}$) can be derived from the calculation written in the Appendix A, and the final equation is expressed as:

$$j_{\text{cat,s}} = \frac{j_{\text{max}}}{1 + \frac{\eta_1^{0.5}}{\frac{k_1^o}{k_c}} + \frac{\frac{K_{\text{O}_2}}{c_{\text{O}_2}}(1 + \eta_1) + \frac{c_{\text{Cu}^{2+}}}{K_{\text{Cu}^{2+}}}\eta_2^{-1}}{1 + \frac{c_{\text{Cu}^{2+}}}{K_{\text{Cu}^{2+}}}}} \quad (5)$$

where j_{max} , k_1^o , k_c , K_{O_2} and $K_{\text{Cu}^{2+}}$ are the maximum catalytic current density, the standard rate constant for the heterogeneous electron transfer between the electrode and the T1 Cu center of CueO, the catalytic constant, and the Michaelis constants of the enzyme for O₂ and Cu²⁺, respectively. To simplify the analysis, the transfer coefficient is assumed to be 0.5 and η_n is expressed as:

$$\eta_n = \exp\left\{\frac{F}{RT}(E - E'^o_n)\right\} \quad (n = 1,2) \quad (6)$$

where E'^o_1 and E'^o_2 are the formal potentials of the T1 Cu center and the Cu²⁺-binding site of CueO, respectively, F is the Faraday constant, R is the gas constant, and T is the absolute temperature. The number of electrons in the rate-determining step involved in the heterogeneous electron transfer was set to 1. The standard rate constant for the heterogeneous electron transfer between the electrode and the Cu²⁺-binding site of CueO ($= k^o_2$) was also defined; however, $j_{\text{cat,s}}$ is independent of k^o_2 . The literature values of K_{O_2} are 0.017 mM for rCueO and 0.012 mM for $\Delta\alpha$ CueO, respectively [45], which are much smaller than c_{O_2} ($= 1.2$ mM) under O₂-saturated conditions. Hence, Eq. (5) can be simplified, as follows:

$$j_{\text{cat,s}} = \frac{j_{\text{max}}}{1 + \frac{\eta_1^{0.5}}{\frac{k_1^o}{k_c}} + \frac{\frac{c_{\text{Cu}^{2+}}}{K_{\text{Cu}^{2+}}}\eta_2^{-1}}{1 + \frac{c_{\text{Cu}^{2+}}}{K_{\text{Cu}^{2+}}}}} \quad (7)$$

To consider the enzyme orientation, then, we distributed three k°_1 values: k°_{\max} (maximum k°), $k^{\circ}_{\max}/10$, and $k^{\circ}_{\max}/10^2$. Moreover, the proportion of k°_1 was set to p_1 , p_2 , and p_3 ($= 1 - p_1 - p_2$), which correspond to k°_{\max} , $k^{\circ}_{\max}/10$, and $k^{\circ}_{\max}/10^2$, respectively. Thus, Eq. (7) can be rewritten as follows:

$$j_{\text{cat},s} = \sum_{n=1}^3 p_n \frac{j_{\max}}{1 + \frac{\eta_1^{0.5}}{\frac{k^{\circ}_{\max}}{k_c} \times 10^{-(n-1)}} + \frac{\frac{C_{\text{Cu}^{2+}}}{K_{\text{Cu}^{2+}}} \eta_2^{-1}}{1 + \frac{C_{\text{Cu}^{2+}}}{K_{\text{Cu}^{2+}}}}} \quad (8)$$

We determined values for the kinetic and thermodynamic parameters using Eq. (8). Firstly, the voltammograms in the absence of Cu^{2+} under O_2 -saturated conditions were fitted to Eq. (8) (Figs. 1A and 1B) using Gnuplot[®], in order to refine $E^{\circ}'_1$, k°_{\max}/k_c , j_{\max} , p_1 , p_2 , and p_3 . The refined data are summarized in Table 1 and the fitted results are shown in Fig. 7. The values of $E^{\circ}'_1$ and $-j_{\max}$ are almost identical for rCueO and $\Delta\alpha\text{CueO}$, while $\Delta\alpha\text{CueO}$ exhibited a larger k°_{\max}/k_c value than rCueO, which indicates that $\Delta\alpha\text{CueO}$ is oriented more favorably for DET on the CNT-NH₂/GC. These results are mostly consistent with those of our previous study in which we investigated DET-type bioelectrocatalysis by CueO at amine-functionalized Ketjen Black-modified electrodes [21].

We also attempted to refine $E^{\circ}'_2$ and $K_{\text{Cu}^{2+}}$ using other fixed parameters ($E^{\circ}'_1$, k°_{\max}/k_c , p_1 , p_2 , and p_3) and j_{cat} values at $t = 30$ s recorded at $E = 0.45, 0.40, 0.35$, and 0.30 V under O_2 -saturated conditions in the presence of Cu^{2+} . Here, j_{\max} was set as to be flexible to account for sample variability. Unfortunately, $E^{\circ}'_2$ and $K_{\text{Cu}^{2+}}$ were unable to be determined owing to parameter flexibility, large j_{cat} errors, and the narrow potential range.

1
2
3 Considering the existence of the unidentified Cu²⁺-binding site in the crystal
4 structure of rCueO elucidated in the presence of 25 mM Cu²⁺ [16], $K_{\text{Cu}^{2+}}$ seems much
5 larger than 1 mM. The CD spectra also suggest that the secondary structure of CueO is
6 almost conserved in the presence of 1 mM Cu²⁺ (Fig. S13), consistent with a large $K_{\text{Cu}^{2+}}$
7 value for CueO. Eq. (8) can be simplified to Eq. (9) when we assume that $c_{\text{Cu}^{2+}} \ll K_{\text{Cu}^{2+}}$:
8
9

$$10 \quad j_{\text{cat},s} = \sum_{n=1}^3 p_n \frac{j_{\text{max}}}{1 + \frac{\eta_1^{0.5}}{\frac{k_{\text{max}}^{\circ}}{k_c} \times 10^{-(n-1)}} + \frac{c_{\text{Cu}^{2+}} \exp\left(-\frac{FE}{RT}\right)}{K_{\text{Cu}^{2+}} \exp\left(-\frac{FE^{\circ'}_2}{RT}\right)}} \quad (9)$$

11
12
13
14
15
16
17
18
19
20
21
22
23 Using Eq. (9), j_{max} and $K_{\text{Cu}^{2+}} \exp\left(-\frac{FE^{\circ'}_2}{RT}\right)$ were refined by GnuPlot[®]. The refined
24 parameters are listed in Table 2. Theoretical steady-state voltammograms for Cu²⁺-
25 dependent reductive inactivation are shown in Fig. 8. While the refined curves
26 successfully reproduce the E - and $c_{\text{Cu}^{2+}}$ -dependent current decreases, the actual $K_{\text{Cu}^{2+}}$ and
27 $E^{\circ'}_2$ values was difficult to determine because of their strong statistical correlation. On
28 the other hand, there seems no significant differences in the values of $K_{\text{Cu}^{2+}} \exp\left(-\frac{FE^{\circ'}_2}{RT}\right)$
29 between rCueO and $\Delta\alpha$ CueO, which is consistent with the hypothesis that Cu²⁺ does not
30 coordinate close to the helical regions but near the TNC and T1 Cu centers.
31
32
33
34
35
36
37
38
39
40
41
42

43 The conformations of the TNC and T1 Cu centers in the ES complex dynamically
44 change during the catalytic cycle [46,47]. Focusing on the mechanism of uncompetitive
45 inhibition, we suggest that the Cu²⁺-binding site is located near the TNC and the T1 Cu
46 centers because only the ES complex appears to be sensitive to Cu²⁺. Three His residues
47 that are generally known to be ligands for Cu^{2+/1+} and other metal cations are present
48 within 16 Å of the TNC center, except for its ligands (His145, His488, and His494 shown
49 in Fig. 9). Consequently, we suggest that Cu²⁺ coordinated to some His residues is
50
51
52
53
54
55
56
57
58
59
60
61
62
63
64
65

1
2
3 electrochemically reduced and induces conformational changes near the TNC center,
4
5 which inhibits the dynamic transitions of the TNC and T1 Cu centers. In particular, the
6
7 crystal structure of rCueO in the presence of 10 mM CuCl₂ shows that His145 is
8
9 coordinated to an additional Cu (referred to as Cu6) [48]. Furthermore, His145 is close to
10
11 His143 and Glu506; the former is a ligand for one of the T3 Cu pair, while the latter is
12
13 suggested to play an important role in the proton relay of the intermediates during the
14
15 catalytic cycle [43]. Hence, we concluded that His145 is the most likely to be a ligand for
16
17 Cu²⁺ which induced the reductive inactivation. The proposed mechanism for the Cu²⁺-
18
19 dependent reductive inactivation of CueO is shown in Scheme 2. More information is
20
21 expected to be obtained by investigating the effects of Cu²⁺ on other DET-type enzymes.
22
23
24
25
26
27
28

29 **4. Conclusions**

30
31 We kinetically and thermodynamically analyzed the Cu²⁺-dependent
32
33 reductive inactivation of the DET-type bioelectrocatalytic activities of rCueO and
34
35 ΔαCueO at NH₂-functionalized MWCNTs. Linear free energy relationships seem to exist
36
37 between the inactivation/reactivation rate constants and the electrode potential, and
38
39 uncompetitive inhibition mechanism appears to operate. We constructed a detailed model
40
41 for reversible inactivation and reactivation, and determined thermodynamic data. Further
42
43 spectroscopic analyses may identify the precise inhibition mechanism. Comparison of
44
45 crystal structures suggest that this Cu²⁺-inactivation process is not exclusively
46
47 encountered in CueO-like proteins, i.e. those enzymes presenting Met-rich domains
48
49 covering the T1 Cu. This suggests that MCOs contain additional copper-binding sites
50
51 other than the T1 Cu and TNC, which can be responsible for catalytic inhibition. Using
52
53 various techniques in spectroscopy, eventually coupled to electrochemistry, biochemistry,
54
55
56
57
58
59
60
61
62
63
64
65

1
2
3 structural biology and theoretical chemistry, a detailed inhibition mechanism focusing on
4
5 intermediates during the catalytic cycle may be elucidated. By combining in vitro studies
6
7 of the effects of Cu^{2+/1+} on MCO-based electrocatalysis and in vivo copper resistance, an
8
9 improved understanding of copper homeostasis in microorganisms is expected. In fine,
10
11 this study can be extended to other copper-efflux enzymes and will lead to the elucidation
12
13 of molecular factors involved in copper homeostasis.
14
15
16
17
18

19 **Acknowledgements**

20
21
22 This work was supported by the sponsorship of JSPS Overseas Challenge
23
24 Program for Young Researchers (to T.A.) and by National Research Agency (ANR,
25
26 France) (N°ANR-21-CE44-0024), CNRS, France. We would like to thank Editage
27
28 (www.editage.com) for English language editing.
29
30
31
32
33

34 **Appendix A. Solution for Eq. (5)**

35
36 Based on the model shown in Scheme 1, the differential equations for the surface
37
38 concentrations of all states of the enzyme ([E_R], [E_O], [ES], [ES-Cu²⁺], and [ES-Cu⁺]) are
39
40 expressed as follows:
41
42

$$43 \frac{d[E_R]}{dt} = -(k_1 + k_{b1})[E_R] + k_{f1}[E_O] + k_{-1}[ES] \quad (A. 1)$$

$$44 \frac{d[E_O]}{dt} = k_{b1}[E_R] - k_{f1}[E_O] + k_c[ES] + k_c[ES-Cu^{2+}] \quad (A. 2)$$

$$45 \frac{d[ES]}{dt} = k_1[E_R] - (k_{-1} + k_c + k_2)[ES] + k_{-2}[ES-Cu^{2+}] \quad (A. 3)$$

$$46 \frac{d[ES-Cu^{2+}]}{dt} = k_2[ES] - (k_c + k_{-2} + k_{f2})[ES-Cu^{2+}] + k_{b2}[ES-Cu^+] \quad (A. 4)$$

$$47 \frac{d[ES-Cu^+]}{dt} = k_{f2}[ES-Cu^{2+}] - k_{b2}[ES-Cu^+] \quad (A. 5)$$

The surface concentration of the total enzyme ($[E_{\text{total}}]$) is defined as:

$$[E_{\text{total}}] = [E_{\text{R}}] + [E_{\text{O}}] + [ES] + [ES-\text{Cu}^{2+}] + [ES-\text{Cu}^+] \quad (\text{A. 6})$$

Under steady-state conditions:

$$\frac{d[E_{\text{R}}]}{dt} = \frac{d[E_{\text{O}}]}{dt} = \frac{d[ES]}{dt} = \frac{d[ES-\text{Cu}^{2+}]}{dt} = \frac{d[ES-\text{Cu}^+]}{dt} = 0 \quad (\text{A. 7})$$

Using (A.1) to (A.7):

$$[ES-\text{Cu}^+] = \frac{k_{\text{f}2}}{k_{\text{b}2}} [ES-\text{Cu}^{2+}] \quad (\text{A. 8})$$

$$[ES] = \left(\frac{k_{\text{c}}}{k_2} + \frac{k_{-2}}{k_2} \right) [ES-\text{Cu}^{2+}] \quad (\text{A. 9})$$

$$[E_{\text{R}}] = \left[\left(\frac{k_{-1}}{k_1} + \frac{k_{\text{c}}}{k_1} \right) \left(\frac{k_{\text{c}}}{k_2} + \frac{k_{-2}}{k_2} \right) + \frac{k_{\text{c}}}{k_1} \right] [ES-\text{Cu}^{2+}] \quad (\text{A. 10})$$

$$[E_{\text{O}}] = \left\{ \frac{k_{\text{b}1}}{k_{\text{f}1}} \left[\left(\frac{k_{-1}}{k_1} + \frac{k_{\text{c}}}{k_1} \right) \left(\frac{k_{\text{c}}}{k_2} + \frac{k_{-2}}{k_2} \right) + \frac{k_{\text{c}}}{k_1} \right] + \frac{k_{\text{c}}}{k_{\text{f}1}} \left(1 + \frac{k_{\text{c}}}{k_2} + \frac{k_{-2}}{k_2} \right) \right\} [ES-\text{Cu}^{2+}] \quad (\text{A. 11})$$

Using (A.6), (A.8), (A.9), (A.10), and (A.11):

$$[ES-\text{Cu}^{2+}] = \frac{[E_{\text{total}}]}{\left(1 + \frac{k_{\text{c}}}{k_{\text{f}1}} \right) \left(1 + \frac{k_{\text{c}}}{k_2} + \frac{k_{-2}}{k_2} \right) + \left[\frac{k_{\text{c}}}{k_1} + \left(\frac{k_{\text{c}}}{k_1} + \frac{k_{-1}}{k_1} \right) \left(\frac{k_{\text{c}}}{k_2} + \frac{k_{-2}}{k_2} \right) \right] \left(1 + \frac{k_{\text{b}1}}{k_{\text{f}1}} \right) + \frac{k_{\text{f}2}}{k_{\text{b}2}}} \quad (\text{A. 12})$$

Here, $j_{\text{cat,s}}$ is ascribed to the catalytic reaction by ES and ES-Cu²⁺, and is expressed as:

$$j_{\text{cat,s}} = n_{\text{O}_2} F k_{\text{c}} ([ES] + [ES-\text{Cu}^{2+}]) = \frac{j_{\text{max}}}{1 + \frac{k_{\text{c}}}{k_{\text{f}1}} + \frac{\left[\frac{k_{\text{c}}}{k_1} + \left(\frac{k_{\text{c}}}{k_1} + \frac{k_{-1}}{k_1} \right) \left(\frac{k_{\text{c}}}{k_2} + \frac{k_{-2}}{k_2} \right) \right] \left(1 + \frac{k_{\text{b}1}}{k_{\text{f}1}} \right) + \frac{k_{\text{f}2}}{k_{\text{b}2}}}{1 + \frac{k_{\text{c}}}{k_2} + \frac{k_{-2}}{k_2}} \quad (\text{A. 13})$$

where the maximum catalytic current density (j_{max}) is defined as:

$$j_{\text{max}} = n_{\text{O}_2} F k_{\text{c}} [E_{\text{total}}] \quad (\text{A. 14})$$

(A.13) can be simplified to:

$$j_{\text{cat,s}} = \frac{j_{\text{max}}}{1 + \frac{k_{\text{c}}}{k_{\text{f}1}} + \frac{\frac{k_{-1}}{k_1} \left[\frac{k_{\text{c}}}{k_{-1}} \frac{k_2}{k_{-2}} + \left(1 + \frac{k_{\text{c}}}{k_{-1}} \right) \left(1 + \frac{k_{\text{c}}}{k_{-2}} \right) \right] \left(1 + \frac{k_{\text{b}1}}{k_{\text{f}1}} \right) + \frac{k_2}{k_{-2}} \frac{k_{\text{f}2}}{k_{\text{b}2}}}{1 + \frac{k_{\text{c}}}{k_{-2}} + \frac{k_2}{k_{-2}}} \quad (\text{A. 13}')$$

Assuming that $\frac{k_{\text{c}}}{k_{-1}} \ll 1$ and $\frac{k_{\text{c}}}{k_{-2}} \ll 1$:

$$j_{\text{cat,s}} = \frac{j_{\text{max}}}{1 + \frac{k_c}{k_{f1}} + \frac{\frac{k_{-1}}{k_1} \left(1 + \frac{k_{b1}}{k_{f1}}\right) + \frac{k_2}{k_{-2}} \frac{k_{f2}}{k_{b2}}}{1 + \frac{k_2}{k_{-2}}} \quad (\text{A. 13''})$$

Here, the kinetic constants can be expressed as:

$$\frac{k_{-1}}{k_1} = \frac{K_{\text{O}_2}}{c_{\text{O}_2}} \quad (\text{A. 15})$$

$$\frac{k_2}{k_{-2}} = \frac{c_{\text{Cu}^{2+}}}{K_{\text{Cu}^{2+}}} \quad (\text{A. 16})$$

$$k_{fn} = k_n^{\circ} \eta_n^{-\alpha_n} \quad (n = 1, 2) \quad (\text{A. 17})$$

$$k_{bn} = k_n^{\circ} \eta_n^{1-\alpha_n} \quad (n = 1, 2) \quad (\text{A. 18})$$

where α_n is the transfer coefficient (assumed to be 0.5) and η_n is defined as:

$$\eta_n = \exp \left\{ \frac{F}{RT} (E - E_n^{\circ'}) \right\} \quad (\text{A. 19})$$

Using (A.15) to (A.19), (A.13'') is re-expressed as:

$$j_{\text{cat,s}} = \frac{j_{\text{max}}}{1 + \frac{\eta_1^{0.5}}{\frac{k_1^{\circ}}{k_c}} + \frac{\frac{K_{\text{O}_2}}{c_{\text{O}_2}} (1 + \eta_1) + \frac{c_{\text{Cu}^{2+}}}{K_{\text{Cu}^{2+}}} \eta_2^{-1}}{1 + \frac{c_{\text{Cu}^{2+}}}{K_{\text{Cu}^{2+}}}}} \quad (\text{A. 13'''})$$

Appendix B. Supplementary data

Supplementary data to this article can be found online at <http://dx.doi.org/XXXXXXXXX>.

References

- [1] E.I. Solomon, U.M. Sundaram, T.E. Machonkin, Multicopper oxidases and oxygenases, *Chem. Rev.* 96 (1996) 2563–2605. <https://doi.org/10.1021/cr950046o>.
- [2] T. Sakurai, K. Kataoka, Basic and applied features of multicopper oxidases, CueO, bilirubin oxidase, and laccase, *Chem. Rec.* 7 (2007) 220–229. <https://doi.org/10.1002/tcr.20125>.
- [3] N. Mano, A. de Poulpiquet, O₂ reduction in enzymatic biofuel cells, *Chem. Rev.* 118 (2018) 2392–2468. <https://doi.org/10.1021/acs.chemrev.7b00220>.
- [4] M. Miyata, Y. Kitazumi, O. Shirai, K. Kataoka, K. Kano, Diffusion limited biosensing of dissolved oxygen by direct electron transfer-type bioelectrocatalysis of multi-copper oxidases immobilized on porous gold microelectrodes. *J. Electroanal. Chem.* 860 (2020) 113895. <https://doi.org/10.1016/j.jelechem.2020.113895>.
- [5] R.D. Milton, S.D. Minteer, Direct enzymatic bioelectrocatalysis: differentiating between myth and reality, *J. R. Soc. Interface* 14 (2017) 20170253. <https://doi.org/10.1098/rsif.2017.0253>.
- [6] N.D.J. Yates, M.A. Fascione, A. Parkin, Methodologies for “wiring” redox proteins/enzymes to electrode surfaces, *Chem. Eur. J.* 24 (2018) 12164–12182. <https://doi.org/10.1002/chem.201800750>.
- [7] M. Sensi, M. del Barrio, C. Baffert, V. Fourmond, C. Léger, New perspectives in hydrogenase direct electrochemistry, *Curr. Opin. Electrochem.* 5 (2017) 135–145. <https://doi.org/10.1016/j.coelec.2017.08.005>.
- [8] F.A. Armstrong, Some fundamental insights into biological redox catalysis from

- 1
2
3 the electrochemical characteristics of enzymes attached directly to electrodes,
4
5 Electrochim. Acta 390 (2021) 138836.
6
7 <https://doi.org/10.1016/j.electacta.2021.138836>.
8
9
- [9] P. Bollella, L. Gorton, R. Antiochia, Direct electron transfer of dehydrogenases for
10 development of 3rd generation biosensors and enzymatic fuel cells, Sensors 18
11 (2018) 1319. <https://doi.org/10.3390/s18051319>.
12
13
14
15
16
- [10] L. Pilan, Tailoring the performance of electrochemical biosensors based on carbon
17 nanomaterials via aryldiazonium electrografting, Bioelectrochemistry 138 (2021)
18 107697. <https://doi.org/10.1016/j.bioelechem.2020.107697>.
19
20
21
22
23
- [11] N. Lalaoui, M. Holzinger, A. Le Goff, S. Cosnier, Diazonium functionalisation of
24 carbon nanotubes for specific orientation of multicopper oxidases: Controlling
25 electron entry points and oxygen diffusion to the enzyme, Chem. Eur. J. 22 (2016)
26 10494–10500. <https://doi.org/10.1002/chem.201601377>.
27
28
29
30
31
32
33
- [12] K. Stolarczyk, D. Łyp, K. Zelechowska, J.F. Biernat, J. Rogalski, R. Bilewicz,
34 Arylated carbon nanotubes for biobatteries and biofuel cells, Electrochim. Acta 79
35 (2012) 74–81. <https://doi.org/10.1016/j.electacta.2012.06.050>.
36
37
38
39
40
- [13] F. Tasca, W. Harreither, R. Ludwig, J.J. Gooding, L. Gorton, Cellobiose
41 dehydrogenase aryl diazonium modified single walled carbon nanotubes: enhanced
42 direct electron transfer through a positively charged surface, Anal. Chem. 83
43 (2011) 3042–3049. <https://doi.org/10.1021/ac103250b>.
44
45
46
47
48
49
- [14] A. Hyre, K. Casanova-Hampton, S. Subashchandrabose, Copper homeostatic
50 mechanisms and their role in the virulence of *Escherichia coli* and *Salmonella*
51 *enterica*, EcoSal Plus, 9 (2020) 0014. <https://doi.org/10.1128/ecosalplus.ESP-0014-2020>.
52
53
54
55
56
57
58
59

- 1
2
3 [15] A. Andrei, Y. Öztürk, B. Khalfaoui-Hassani, J. Rauch, D. Marckmann, P.-I.
4
5 Trasnea, F. Daldal, H.-G. Koch, Cu homeostasis in bacteria: the ins and outs,
6
7 Membranes 10 (2020) 242. <https://doi.org/10.3390/membranes10090242>.
8
9
- 10 [16] S.K. Singh, S.A. Roberts, S.F. McDevitt, A. Weichsel, G.F. Wildner, G.B. Grass,
11
12 C. Rensing, W.R. Montfort, Crystal structures of multicopper oxidase CueO bound
13
14 to copper(I) and silver(I): functional role of a methionine-rich sequence, J. Biol.
15
16 Chem. 286 (2011) 37849–37857. <https://doi.org/10.1074/jbc.M111.293589>.
17
18
- 19 [17] I. Mazurenko, T. Adachi, B. Ezraty, M. Ilbert, K. Sowa, E. Lojou, Electrochemistry
20
21 of copper efflux oxidase-like multicopper oxidases involved in copper
22
23 homeostasis, Curr. Opin. Electrochem. 32 (2022) 100919.
24
25 <https://doi.org/10.1016/j.coelec.2021.100919>.
26
27
- 28 [18] K. Kataoka, H. Komori, Y. Ueki, Y. Konno, Y. Kamitaka, S. Kurose, S. Tsujimura,
29
30 Y. Higuchi, K. Kano, D. Seo, T. Sakurai, Structure and function of the engineered
31
32 multicopper oxidase CueO from *Escherichia coli*—Deletion of the methionine-rich
33
34 helical region covering the substrate-binding site, J. Mol. Biol. 373 (2007) 141–
35
36 152. <https://doi.org/10.1016/j.jmb.2007.07.041>.
37
38
- 39 [19] S. Kurose, K. Kataoka, K. Otsuka, Y. Tsujino, T. Sakurai, Promotion of laccase
40
41 activities of *Escherichia coli* cuprous oxidase, CueO by deleting the segment
42
43 covering the substrate binding site, Chem. Lett. 36 (2007) 232–233.
44
45 <https://doi.org/10.1246/cl.2007.232>.
46
47
- 48 [20] S.A. Roberts, G.F. Wildner, G. Grass, A. Weichsel, A. Ambrus, C. Rensing, W.R.
49
50 Montfort, A labile regulatory copper ion lies near the T1 copper site in the
51
52 multicopper oxidase CueO, J. Biol. Chem. 278 (2003) 31958–31963.
53
54 <https://doi.org/10.1074/jbc.M302963200>.
55
56
57
58
59
60
61
62
63
64
65

- 1
2
3 [21] T. Adachi, Y. Kitazumi, O. Shirai, T. Kawano, K. Kataoka, K. Kano, Effects of
4 elimination of α helix regions on direct electron transfer-type bioelectrocatalytic
5 properties of copper efflux oxidase, *Electrochemistry* 88 (2020) 185–189.
6
7 <https://doi.org/10.5796/electrochemistry.20-00015>.
8
9
10
11
12 [22] V.P. Hitaishi, R. Clément, L. Quattrocchi, P. Parent, D. Duché, L. Zuily, M. Ilbert,
13 E. Lojou, I. Mazurenko, Interplay between orientation at electrodes and copper
14 activation of *Thermus thermophilus* laccase for O₂ reduction, *J. Am. Chem. Soc.*
15 142 (2020) 1394–1405. <https://doi.org/10.1021/jacs.9b11147>.
16
17
18
19
20
21 [23] M. Valles, A.F. Kamaruddin, L.S. Wong, C.F. Blanford, Inhibition in multicopper
22 oxidases: a critical review, *Catal. Sci. Technol.* 10 (2020) 5386–5410.
23
24 <https://doi.org/10.1039/D0CY00724B>.
25
26
27
28 [24] R. Antiochia, D. Oyarzun, J. Sánchez, F. Tasca, Comparison of direct and mediated
29 electron transfer for bilirubin oxidase from *Myrothecium verrucaria*. Effects of
30 inhibitors and temperature on the oxygen reduction reaction, *Catalysts* 9 (2019)
31 1056. <https://doi.org/10.3390/catal9121056>.
32
33
34
35
36
37
38 [25] A. de Poulpiquet, C.H. Kjaergaard, J. Rouhana, I. Mazurenko, P. Infossi, S.
39 Gounel, R. Gadiou, M.T. Giudici-Ortoni, E.I. Solomon, N. Mano, E. Lojou,
40 Mechanism of chloride inhibition of bilirubin oxidases and its dependence on
41 potential and pH, *ACS Catal.* 7 (2017) 3916–3923.
42
43 <https://doi.org/10.1021/acscatal.7b01286>.
44
45
46
47
48
49 [26] F. Tasca, D. Farias, C. Castro, C. Acuna-Rougier, R. Antiochia, Bilirubin oxidase
50 from *Myrothecium verrucaria* physically absorbed on graphite electrodes. Insights
51 into the alternative resting form and the sources of activity loss, *PLoS ONE* 10
52 (2015) e0132181. <https://doi.org/10.1371/journal.pone.0132181>.
53
54
55
56
57
58
59
60
61
62
63
64
65

- 1
2
3 [27] C.H. Kjaergaard, F. Durand, F. Tasca, M.F. Qayyum, B. Kauffmann, S. Gounel,
4
5 E. Suraniti, K.O. Hodgson, B. Hedman, N. Mano, E.I. Solomon, Spectroscopic and
6
7 crystallographic characterization of “alternative resting” and “resting oxidized”
8
9 enzyme forms of bilirubin oxidase: Implications for activity and electrochemical
10
11 behavior of multicopper oxidases, *J. Am. Chem. Soc.* 134 (2012) 5548–5551.
12
13 <https://doi.org/10.1021/ja211872j>.
14
15
16 [28] J. Hirose, K. Inoue, H. Sakuragi, M. Kikkawa, M. Minakami, T. Morikawa, H.
17
18 Iwamoto, K. Hiromi, Anions binding to bilirubin oxidase from *Trachyderma*
19
20 *tsunodae* K-2593, *Inorganica Chim. Acta* 273 (1998) 204–212.
21
22 [https://doi.org/10.1016/S0020-1693\(97\)06183-5](https://doi.org/10.1016/S0020-1693(97)06183-5).
23
24
25 [29] S. Gounel, J. Rouhana, C. Stines-Chaumeil, M. Cadet, N. Mano, Increasing the
26
27 catalytic activity of Bilirubin oxidase from *Bacillus pumilus*: Importance of host
28
29 strain and chaperones proteins, *J. Biotechnol.* 230 (2016) 19–25.
30
31 <https://doi.org/10.1016/j.jbiotec.2016.04.035>.
32
33
34 [30] K.A. Vincent, A. Parkin, F.A. Armstrong, Investigating and exploiting the
35
36 electrocatalytic properties of hydrogenases, *Chem. Rev.* 107 (2007) 4366–4413.
37
38 <https://doi.org/10.1021/cr050191u>.
39
40
41 [31] K. So, R. Hamamoto, R. Takeuchi, Y. Kitazumi, O. Shirai, R. Endo, H. Nishihara,
42
43 Y. Higuchi, K. Kano, Bioelectrochemical analysis of thermodynamics of the
44
45 catalytic cycle and kinetics of the oxidative inactivation of oxygen-tolerant [NiFe]-
46
47 hydrogenase, *J. Electroanal. Chem.* 766 (2016) 152–161.
48
49 <https://doi.org/10.1016/j.jelechem.2016.02.009>.
50
51
52 [32] V. Ducros, A.M. Brzozowski, K.S. Wilson, S.H. Brown, P. Østergaard, P.
53
54 Schneider, D.S. Yaver, A.H. Pedersen, G.J. Davies, Crystal structure of the type-2
55
56
57
58
59
60
61
62
63
64
65

- 1
2
3 Cu depleted laccase from *Coprinus cinereus* at 2.2 Å resolution, Nat. Struct. Biol.
4
5 5 (1998) 310–316. <https://doi.org/10.1038/nsb0498-310>.
6
7
8 [33] N. Hakulinen, L.-L. Kiiskinen, K. Kruus, M. Saloheimo, A. Paananen, A. Koivula,
9
10 J. Rouvinen, Crystal structure of a laccase from *Melanocarpus albomyces* with an
11
12 intact trinuclear copper site, Nat. Struct. Biol. 9 (2002) 601–605.
13
14 <https://doi.org/10.1038/nsb823>.
15
16
17 [34] K. Piontek, M. Antorini, T. Choinowski, Crystal structure of a laccase from the
18
19 fungus *Trametes versicolor* at 1.90-Å resolution containing a full complement of
20
21 coppers, J. Biol. Chem. 277 (2002) 37663–37669.
22
23 <https://doi.org/10.1074/jbc.M204571200>.
24
25
26 [35] X. Li, Z. Wei, M. Zhang, X. Peng, G. Yu, M. Teng, W. Gong, Crystal structures
27
28 of *E. coli* laccase CueO at different copper concentrations, Biochem. Biophys. Res.
29
30 Commun. 354 (2007) 21–26. <https://doi.org/10.1016/j.bbrc.2006.12.116>.
31
32
33 [36] A.J. Bard, R. Parsons, J. Jordan, Standard potential in aqueous solution, Marcel
34
35 Dekker (1985). <https://doi.org/10.1201/9780203738764>.
36
37
38 [37] F. Xu, W. Shin, S.H. Brown, J.A. Wahleithner, U.M. Sundaram, E.I. Solomon, A
39
40 study of a series of recombinant fungal laccases and bilirubin oxidase that exhibit
41
42 significant differences in redox potential, substrate specificity, and stability,
43
44 Biochem. Biophys. Acta 1292 (1996) 303–311. [https://doi.org/10.1016/0167-
45
46 4838\(95\)00210-3](https://doi.org/10.1016/0167-4838(95)00210-3).
47
48
49 [38] R. Clément, X. Wang, F. Biaso, M. Ilbert, I. Mazurenko, E. Lojou, Mutations in
50
51 the coordination spheres of T1 Cu affect Cu²⁺-activation of the laccase from
52
53 *Thermus thermophilus*, Biochimie 182 (2021) 228–237.
54
55 <https://doi.org/10.1016/j.biochi.2021.01.006>.
56
57
58
59
60
61
62
63
64
65

- 1
2
3 [39] A.A. Hamdan, P.-P. Liebgott, V. Fourmond, O. Gutiérrez-Sanz, A.L. De Lacey, P.
4
5 Infossi, M. Rousset, S. Dementin, C. Léger, Relation between anaerobic
6
7 inactivation and oxygen tolerance in a large series of NiFe hydrogenase mutants,
8
9 Proc. Natl. Acad. Sci. USA 109 (2012) 19916–19921.
10
11 <https://doi.org/10.1073/pnas.1212258109>.
12
13
14 [40] D.M. Himmelblau, Diffusion of dissolved gases in liquids. Chem. Rev. 64 (1964)
15
16 527–550. <https://doi.org/10.1021/cr60231a002>.
17
18
19 [41] A. Nagashima, Viscosity of water substance—new international formulation and its
20
21 background, J. Phys. Chem. Ref. Data 6 (1977) 1133–1166.
22
23 <https://doi.org/10.1063/1.555562>.
24
25
26 [42] IUPAC Solubility Data Series (Ed. R. Battino), “Oxygen and Ozone”, Vol. 7,
27
28 Pergamon Press, Oxford (1981).
29
30
31 [43] P.J. Butterworth, The use of dixon plots to study enzyme inhibition, Biochim.
32
33 Biophys. Acta 289 (1972) 251–253. [https://doi.org/10.1016/0005-2744\(72\)90074-](https://doi.org/10.1016/0005-2744(72)90074-5)
34
35 [5](https://doi.org/10.1016/0005-2744(72)90074-5).
36
37
38 [44] G.A. Grant, The many faces of partial inhibition: Revealing imposters with
39
40 graphical analysis, Arch. Biochem. Biophys. 653 (2018) 10–23.
41
42 <https://doi.org/10.1016/j.abb.2018.06.009>.
43
44
45 [45] K. Kataoka, T. Sakurai, Role of hydrogen bond connecting ligands for substrate
46
47 and type I copper in copper(I) oxidase CueO, Chem. Lett. 42 (2013) 1102–1104.
48
49 <https://doi.org/10.1246/cl.130422>.
50
51
52 [46] E.I. Solomon, A.J. Augustine, J. Yoon, O₂ reduction to H₂O by the multicopper
53
54 oxidases, Dalton Trans. 30 (2008) 3921–3932. <https://doi.org/10.1039/B800799C>.
55
56
57 [47] H. Komori, R. Sugiyama, K. Kataoka, Y. Higuchi, T. Sakurai, An O-centered
58
59

1
2
3 structure of the trinuclear copper center in the Cys500Ser/Glu506Gln mutant of
4
5 CueO and structural changes in low to high X-ray dose conditions, *Angew. Chem.*
6
7 *Int. Ed.* 51 (2012) 1–5. <https://doi.org/10.1002/anie.201107739>.
8
9

- 10 [48] H. Wang, X. Liu, J. Zhao, Q. Yue, Y. Yan, Z. Gao, Y. Dong, Z. Zhang, Y. Fan, J.
11
12 Tian, N. Wu, Y. Gong, Crystal structures of multicopper oxidase CueO G304K
13
14 mutant: structural basis of the increased laccase activity, *Sci. Rep.* 8 (2018) 14252.
15
16 <https://doi.org/10.1038/s41598-018-32446-7>.
17
18
19
20
21
22
23
24
25
26
27
28
29
30
31
32
33
34
35
36
37
38
39
40
41
42
43
44
45
46
47
48
49
50
51
52
53
54
55
56
57
58
59
60
61
62
63
64
65

1
2
3 **Figure captions**
4

5
6 Figure 1. (A) CVs for O₂ reduction at (A) rCueO- and (B) ΔαCueO-modified CNT-
7 NH₂/GCs in 0.1 M acetate buffer (pH 5.0) at 25 °C in an O₂-saturated atmosphere at a
8 scan rate (ν) of 5 mV s⁻¹ and $\omega = 4000$ rpm (broken lines). The solid lines correspond to
9 CVs recorded in the presence of CuSO₄ at the concentration indicated at the left of each
10 curve. The dotted red lines correspond to CVs recorded in a N₂-saturated atmosphere in
11 the absence of CuSO₄. The insets show enlarged voltammograms.
12
13
14
15
16
17
18
19
20
21

22
23 Figure 2. CVs at various scan rates recorded at the rCueO-modified CNT-NH₂/GC in 0.1
24 M acetate buffer (pH 5.0) containing 0.5 mM CuSO₄ at 25 °C in an O₂-saturated
25 atmosphere at $\omega = 4000$ rpm. The scan rate is indicated at left of each curve. The broken
26 line corresponds to the CV recorded in the absence of CuSO₄ at $\nu = 5$ mV s⁻¹.
27
28
29
30
31

32
33
34 Figure 3. Multi-scanned CVs at the rCueO-modified CNT-NH₂/GC in 0.1 M acetate
35 buffer (pH 5.0) containing 1 mM CuSO₄ at 25 °C in an O₂-saturated atmosphere at $\nu =$
36 10 mV s⁻¹ and $\omega = 4000$ rpm (solid lines), swept to the lowest potentials of (A) 0.3 V and
37 (B) 0.2 V. The broken lines correspond to CVs recorded in the absence of CuSO₄. The
38 dotted lines correspond to CVs recorded at the CNT-NH₂/GC without enzyme
39 modifications in the presence of 1 mM CuSO₄. The insets show enlarged voltammograms.
40
41
42
43
44
45
46
47
48
49
50

51 Figure 4. CAs at (A) rCueO- and (B) ΔαCueO-modified CNT-NH₂/GCs in 0.1 M acetate
52 buffer (pH 5.0) at 25 °C in an O₂-saturated atmosphere at $\omega = 4000$ rpm and $E = 0.35$ V,
53 in the presence of CuSO₄ at concentrations indicated at the right of each curve. The open
54 circles and dotted lines correspond to experimental and refined values, respectively.
55
56
57
58
59
60
61
62
63
64
65

1
2
3
4
5 Figure 5. Refined k_I and k_A values for rCueO (circles) and $\Delta\alpha$ CueO (squares). (A, B)
6 Relationships between the potential and the common logarithms of k_I and k_A in the
7 presence of 1 mM CuSO₄, respectively. (C, D) Relationships between k_I and k_A , and the
8 CuSO₄ concentration at 0.35 V, respectively. Error bars were evaluated using Student's t -
9 distributions at a 90% confidence level ($n = 5$).
10
11
12
13
14
15
16
17
18

19 Figure 6. Lineweaver–Burk and Dixon plots for (A, B) rCueO and (C, D) $\Delta\alpha$ CueO at $E =$
20 0.35 V. Error bars were evaluated using Student's t -distributions at a 90% confidence
21 level ($n = 5$). The dotted lines indicate regression lines.
22
23
24
25
26
27
28

29 Figure 7. Linear sweep voltammograms for O₂ reduction at rCueO- (circles) and $\Delta\alpha$ CueO-
30 (squares) modified CNT-NH₂/GCs in 0.1 M acetate buffer (pH 5.0) at 25 °C in an O₂-
31 saturated atmosphere at $\omega = 4000$ rpm, in the absence of Cu²⁺. The dotted lines correspond
32 to refined curves determined by non-linear regression analysis based on Eq. (8).
33
34
35
36
37
38
39
40
41

42 Figure 8. Steady-state current densities for Cu²⁺-dependent reductive inactivation at (A)
43 rCueO- and (B) $\Delta\alpha$ CueO-modified CNT-NH₂/GCs in 0.1 M acetate buffer (pH 5.0) at 25
44 °C in an O₂-saturated atmosphere at $\omega = 4000$ rpm. Errors were evaluated using Student's
45 t -distributions at a 90% confidence level ($n = 5$). The dotted lines correspond to refined
46 curves determined by non-linear regression analysis based on Eq. (9).
47
48
49
50
51
52
53
54
55

56 Figure 9. Crystal structures of rCueO (A; PDB: 3OD3) and $\Delta\alpha$ CueO (B; PDB: 2YXV).
57
58
59
60
61
62
63
64
65

1
2
3 Scheme 1. Proposed model for the Cu^{2+} -dependent reductive inactivation of CueO.
4

5 Notations:
6

7 E_R : the reduced state of the enzyme
8

9 E_O : the oxidized state of the enzyme
10

11 ES : the enzyme-substrate complex
12

13 $ES\text{-Cu}^{2+}$: the active state of the enzyme-substrate-inhibitor complex
14

15 $ES\text{-Cu}^+$: the inactive state of the enzyme-substrate-inhibitor complex
16

17 k_c : the catalytic constant
18

19 k_1 : the kinetic constant of coordination between the enzyme and the substrate
20

21 k_{-1} : the kinetic constant of dissociation between the enzyme and the substrate
22

23 k_{f1} : the forward electrode kinetic constant of the electrode-active site of the enzyme
24

25 k_{b1} : the backward electrode kinetic constant of the electrode-active site of the enzyme
26

27 k_2 : the kinetic constant of coordination between the enzyme and the inhibitor
28

29 k_{-2} : the kinetic constant of dissociation between the enzyme and the inhibitor
30

31 k_{f2} : the forward electrode kinetic constant of the inhibitor-binding site of the enzyme
32

33 k_{b2} : the backward electrode kinetic constant of the inhibitor-binding site of the enzyme
34

35
36
37
38
39
40
41
42
43 Scheme 2. Proposed mechanism for the Cu^{2+} -dependent reductive inactivation of CueO.
44
45
46
47
48
49
50
51
52
53
54
55
56
57
58
59
60
61
62
63
64
65

1
2
3
4
5
6
7
8
9
10
11
12
13
14
15
16
17
18
19
20
21
22
23
24
25
26
27
28
29
30
31
32
33
34
35
36
37
38
39
40
41
42
43
44
45
46
47
48
49
50
51
52
53
54
55
56
57
58
59
60
61
62
63
64
65

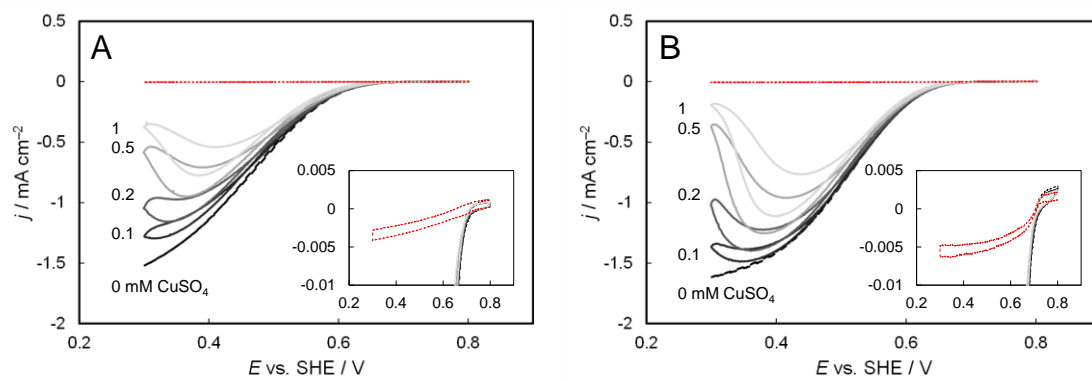


Figure 1.

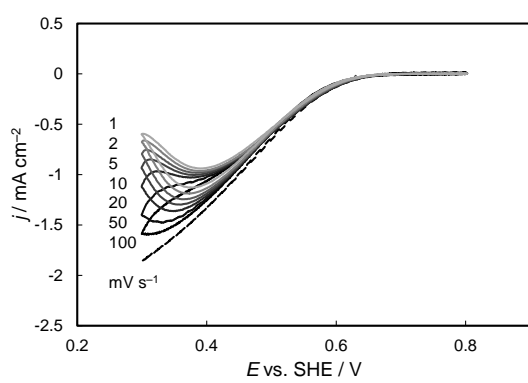


Figure 2.

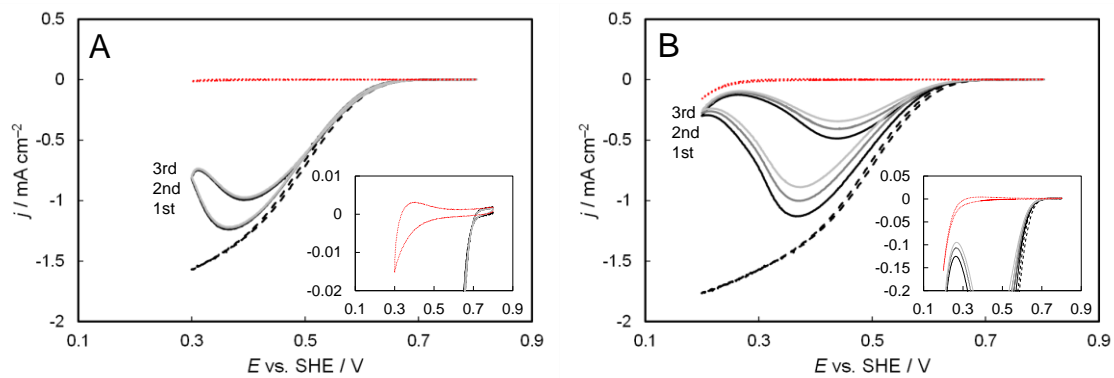


Figure 3.

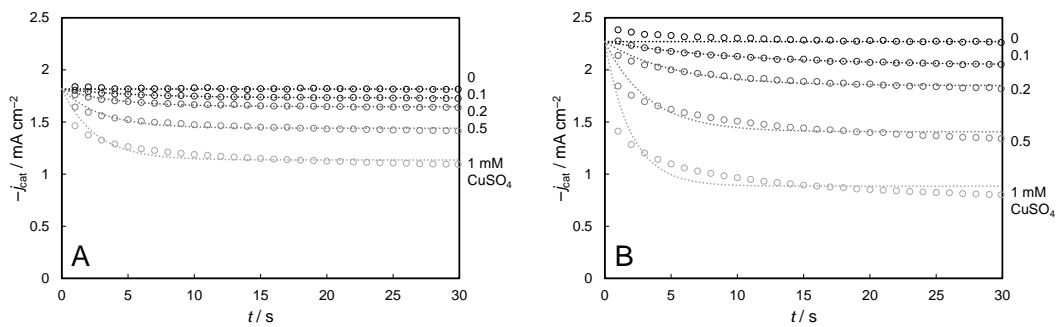


Figure 4.

1
2
3
4
5
6
7
8
9
10
11
12
13
14
15
16
17
18
19
20
21
22
23
24
25
26
27
28
29
30
31
32
33
34
35
36
37
38
39
40
41
42
43
44
45
46
47
48
49
50
51
52
53
54
55
56
57
58
59
60
61
62
63
64
65

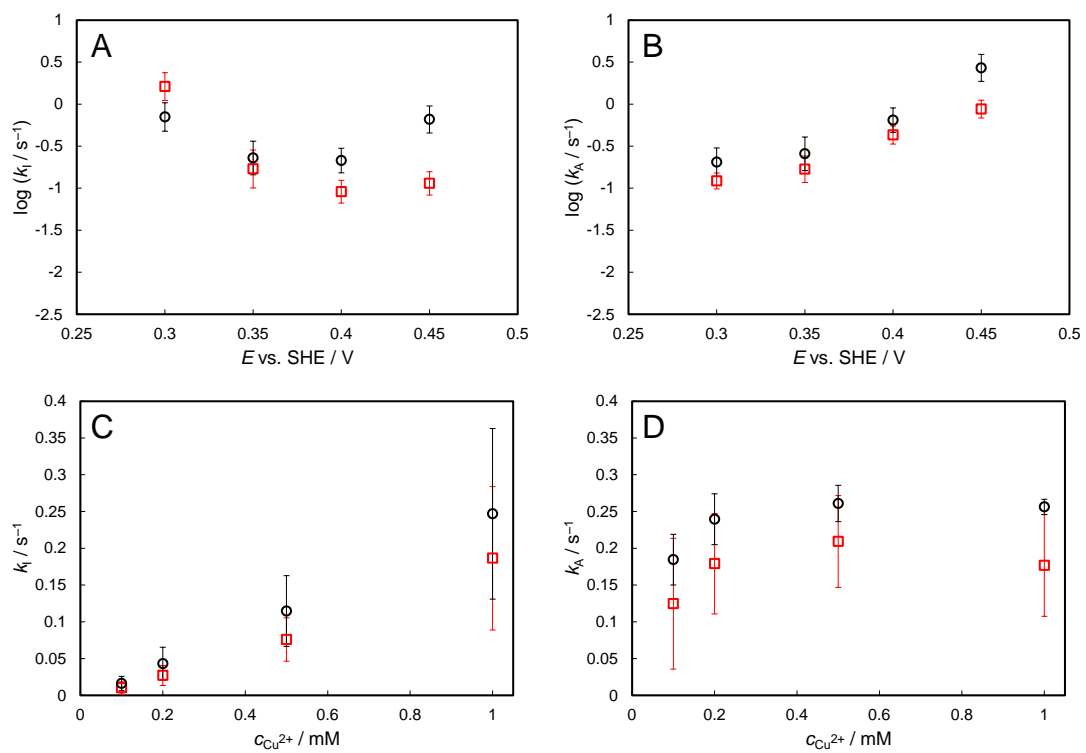


Figure 5.

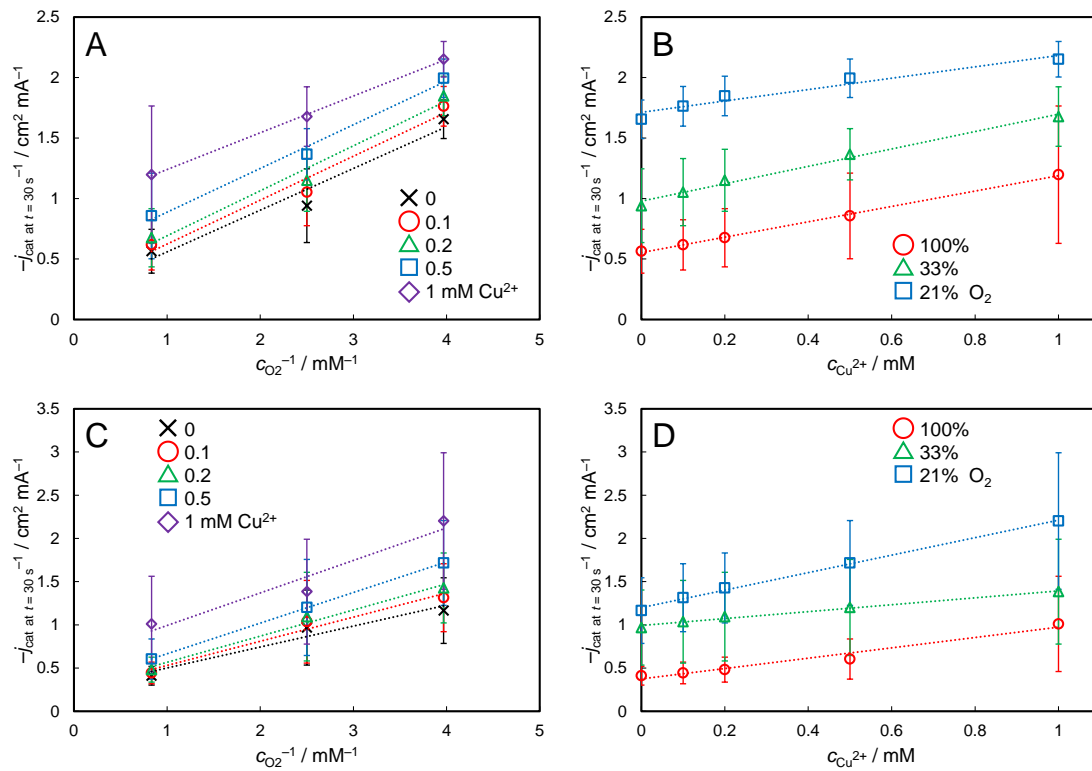


Figure 6.

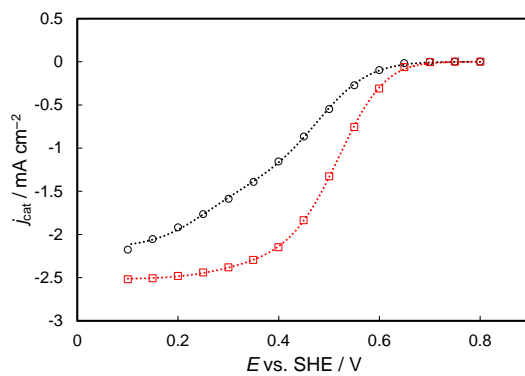


Figure 7.

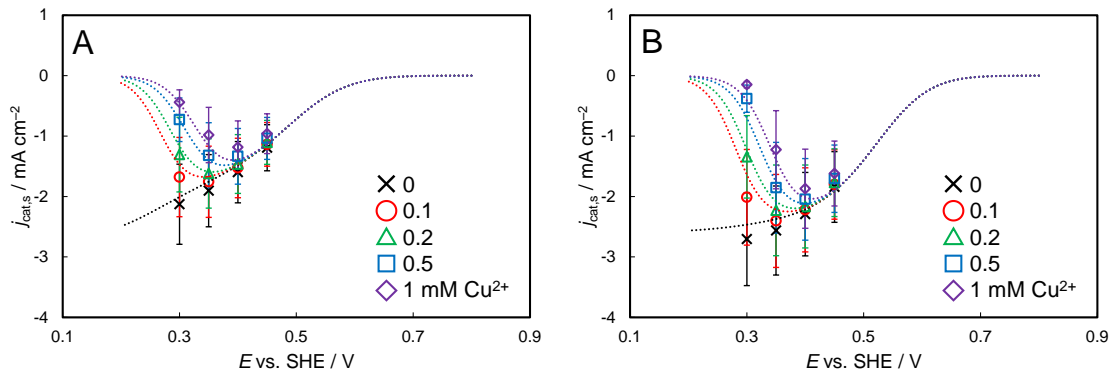


Figure 8.

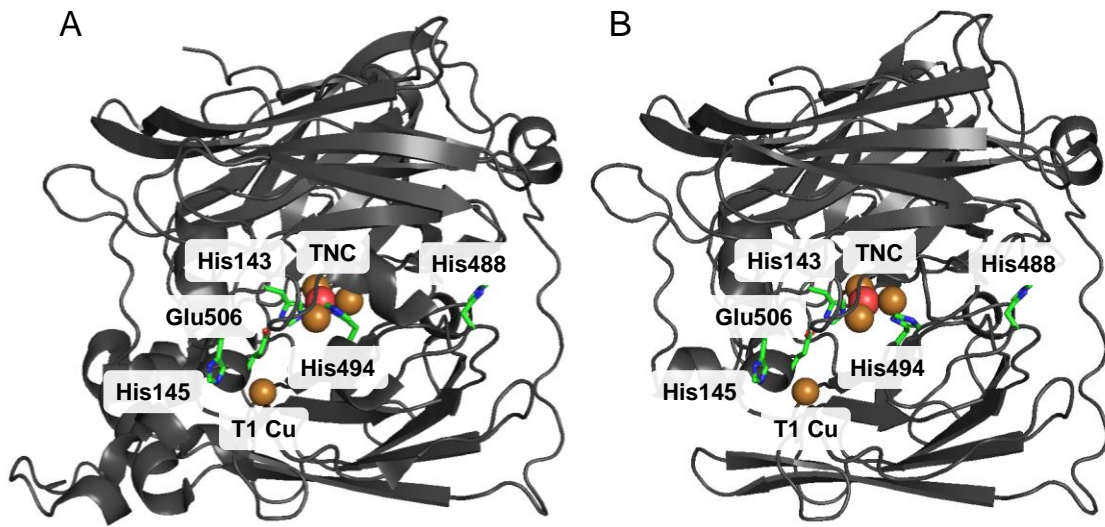
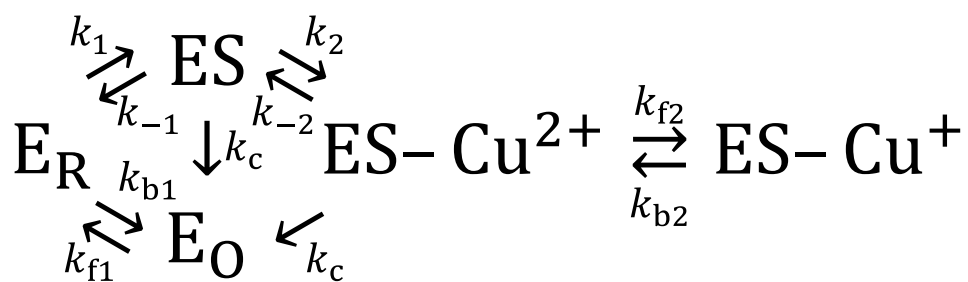
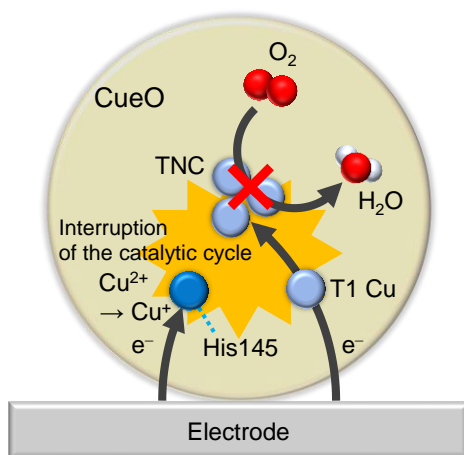


Figure 9.



Scheme 1.



Scheme 2.

Table 1. Refined data obtained by the non-linear regression analyses of voltammograms. Errors were evaluated from Student's t -distribution at a 90% confidence level ($n = 5$).

	$E^{\circ'}_1 / \text{V}$	$k^{\circ}_{\text{max}} / k_{\text{c}}$	$-j_{\text{max}} / \text{mA cm}^{-2}$	p_1	p_2	p_3
rCueO	0.465 ± 0.007	1.6 ± 0.7	2.3 ± 0.3	0.6 ± 0.1	0.10 ± 0.05	0.3 ± 0.1
$\Delta\alpha\text{CueO}$	0.464 ± 0.003	3.0 ± 0.6	2.6 ± 0.4	0.91 ± 0.03	0.03 ± 0.03	0.06 ± 0.03

Table 2. Refined data obtained by the non-linear regression analyses of j_{cat} values at $t = 30$ s. Errors were evaluated from Student's t -distribution at a 90% confidence level ($n = 5$).

	$-j_{\text{max}} / \text{mA cm}^{-2}$	$K_{\text{Cu}^{2+}} \exp\left(-\frac{F}{RT} E^{\circ'}_2\right) / \text{mM}$
rCueO	2.8 ± 0.9	$(1.9 \pm 0.7) \times 10^{-6}$
$\Delta\alpha\text{CueO}$	2.6 ± 0.8	$(1.6 \pm 0.7) \times 10^{-6}$